Supporting information

Two-Step Construction of KPDMS/Al_2O_3 Ultra-Barriers for Wearable Sensors

Di wen, Ruige Yuan, Fan Yang*, Rong Chen*

State Key Laboratory of Intelligent Manufacturing Equipment and Technology of School of Mechanical Science and Engineering, Huazhong University of Science and Technology, Wuhan 430074, China

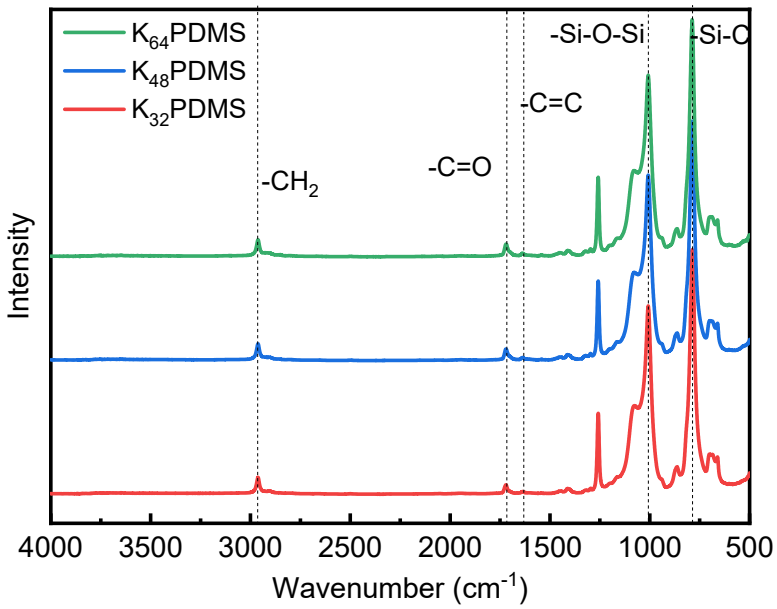

Figure S1. The FTIR of pristine K_nPDMS (n=32, 48, 64).

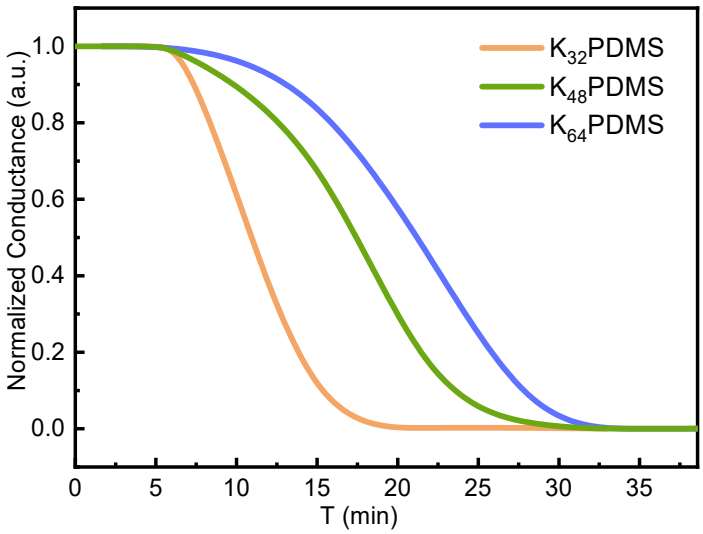

Figure S2. The barrier property of pristine K_nPDMS

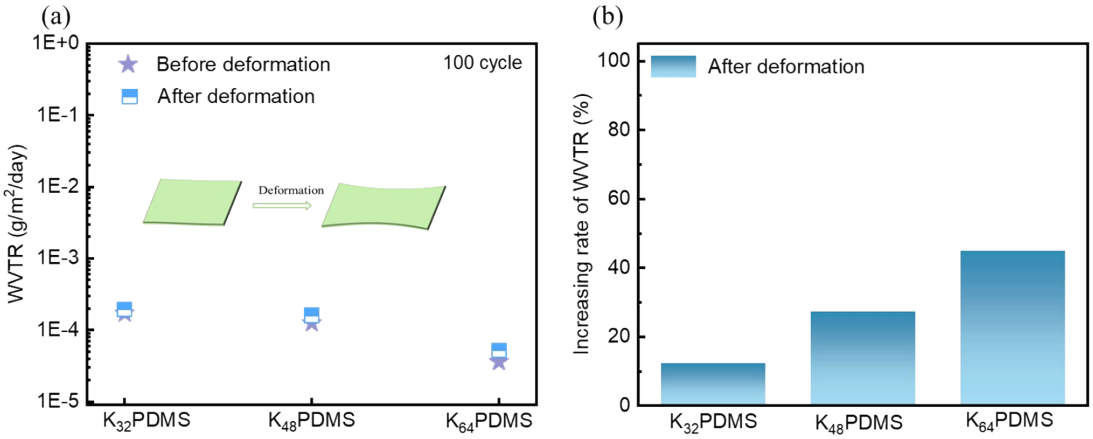

Figure S3. The barrier property of K_nPDMS with 100 ALI cycles, UV-curing for 1 minute, before and after stretching, at a tensile strain of 1%. (a) Change in WVTR. (b) Increasing rate of WVTR.

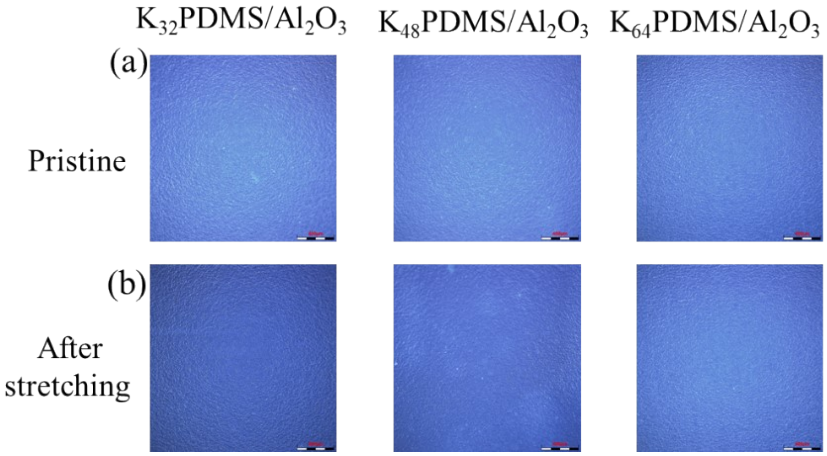

Figure S4. The morphology of K_nPDMS (n=32, 48, 64) barriers with 100 ALI cycles before and after stretching at 1% strain.

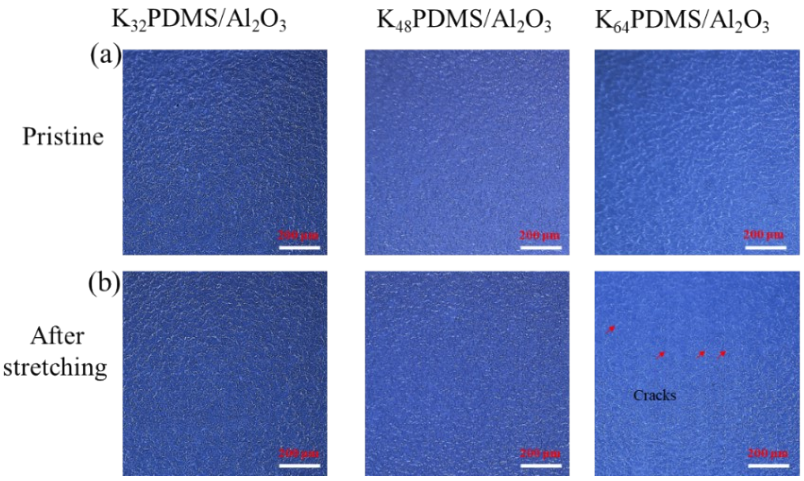

Figure S5. The morphology of K_nPDMS (n=32, 48, 64) barriers with 130 ALI cycles before and after stretching at 1% strain.

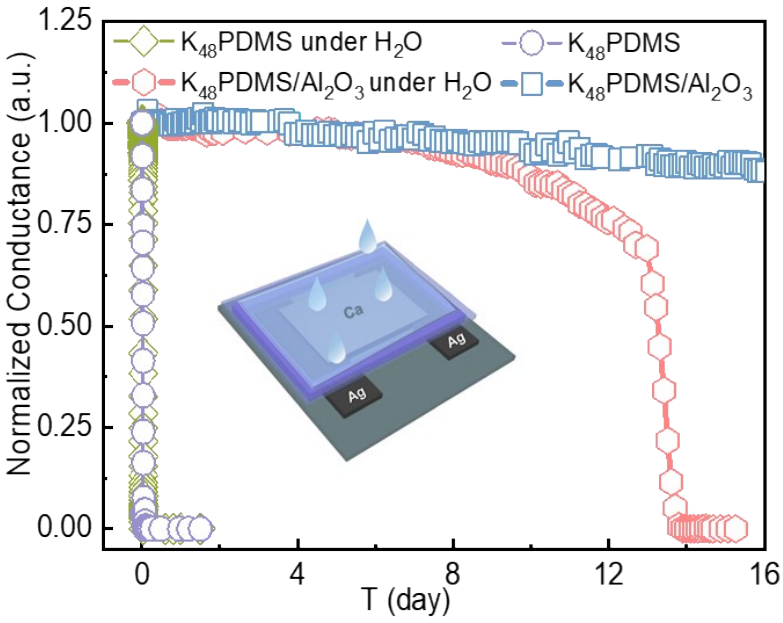

Figure S6. Stability testing of encapsulated Ca devices with/without H_2O. Inset: Diagram of the Ca device.

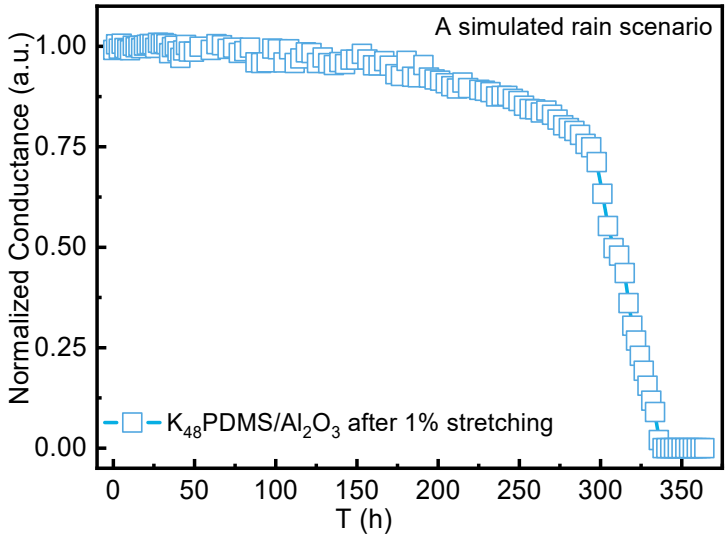

Figure S7. The barrier property of $K_{48}PDMS/Al_2O_3$ encapsulated Ca devices when exposed to intermittent water.

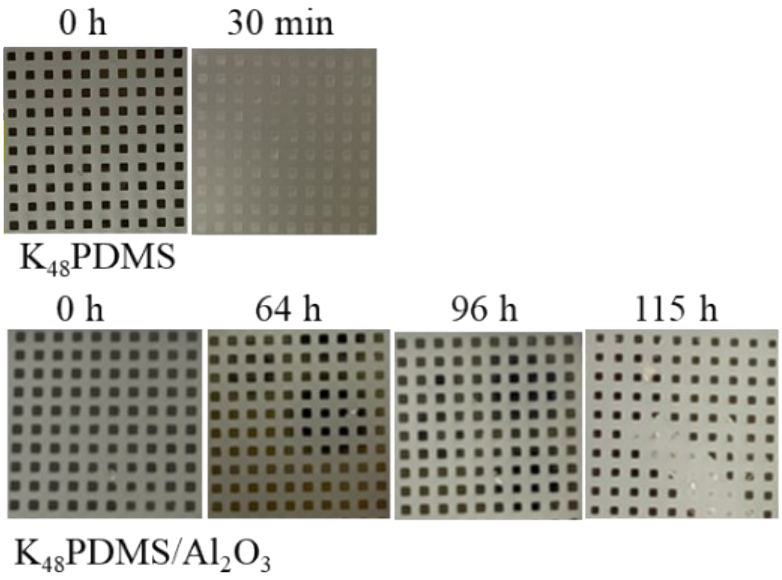

Figure S8. Normalized conductance of encapsulated Ca device with/without H_2O at 25 °C/50 % RH.

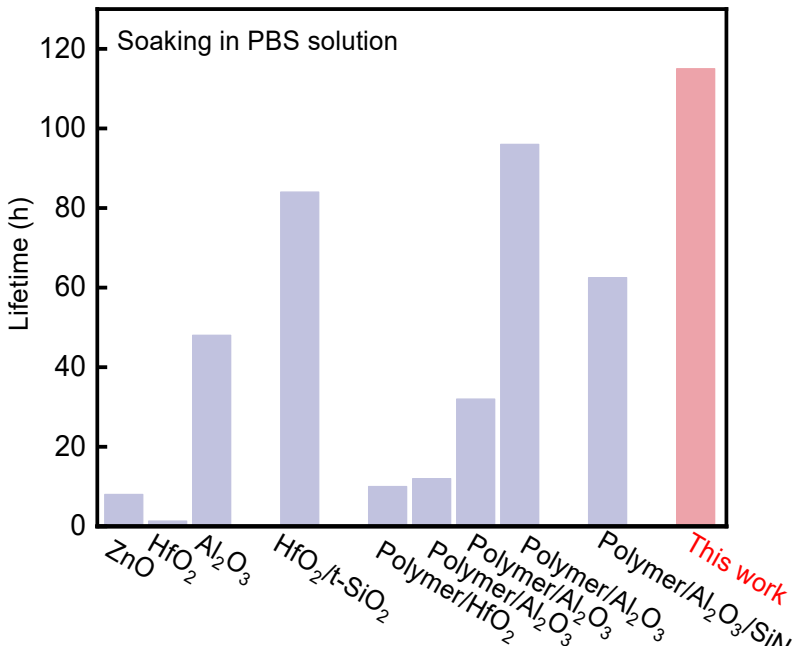

Figure S9. Literature summary of resistance to PBS solution for various barriers fabricated by ALD

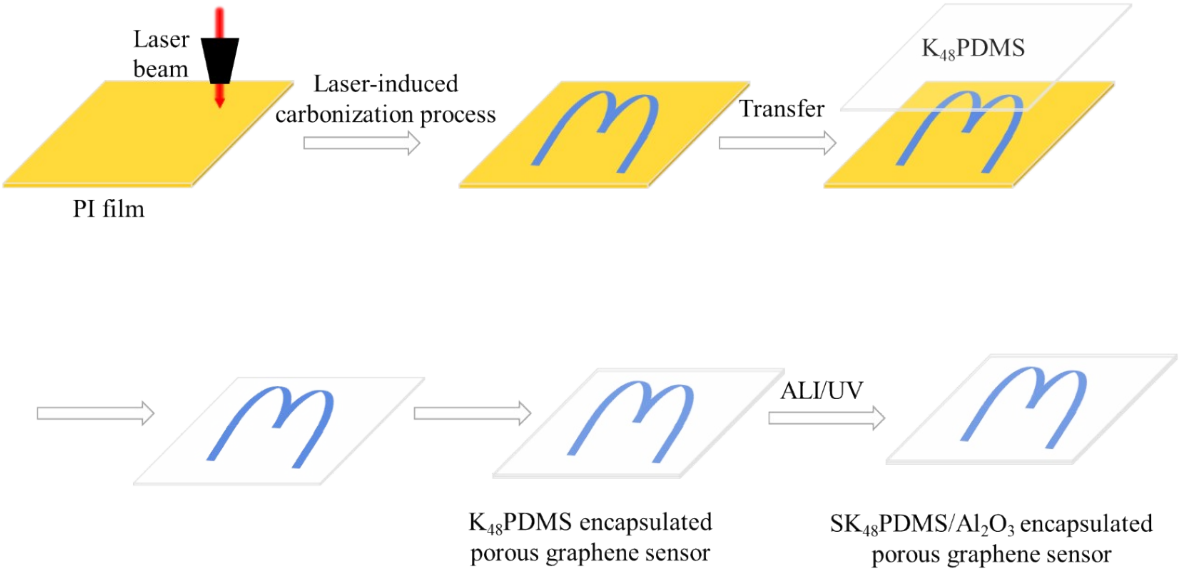

Figure S10. The synthetic route of $K_{48}PDMS/Al_2O_3$ encapsulated porous graphene sensor involves employing porous graphene as the electrode material.

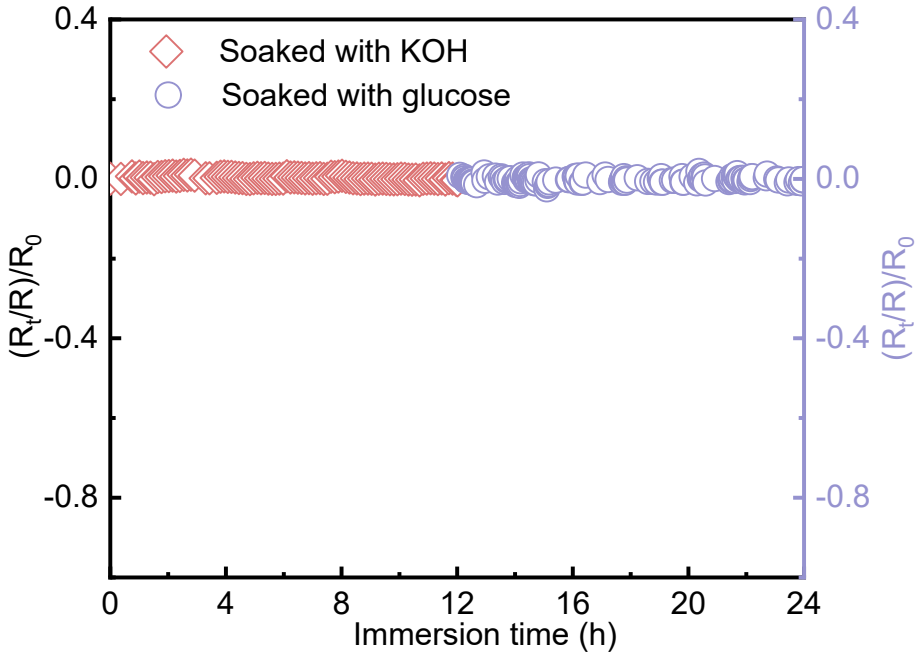

Figure S11. Relative resistance variation of $K_{48}PDMS/Al_2O_3$ encapsulated stretchable sensor soaked with the KOH and glucose.

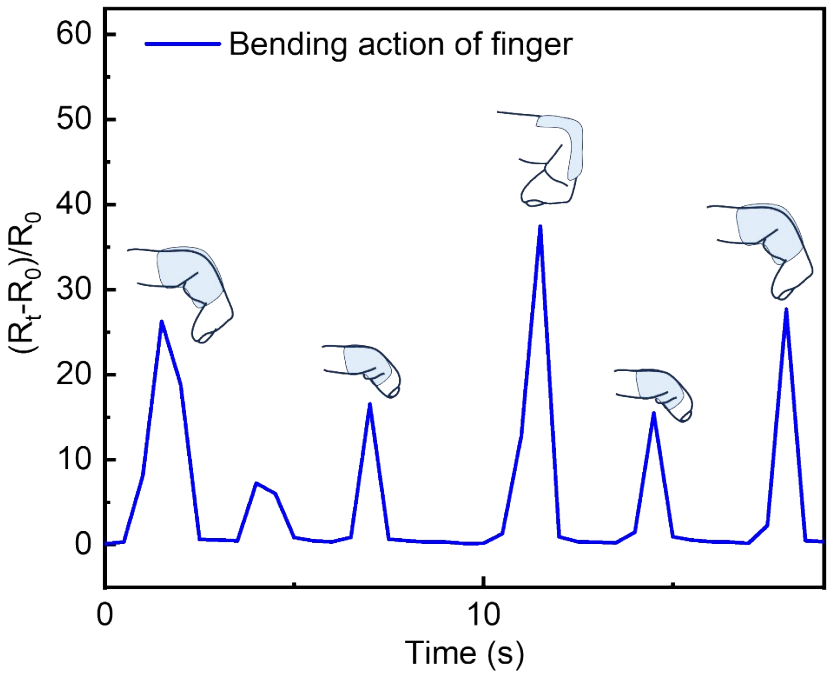

Figure S12. Response of encapsulated sensor to different bending actions of a human finger

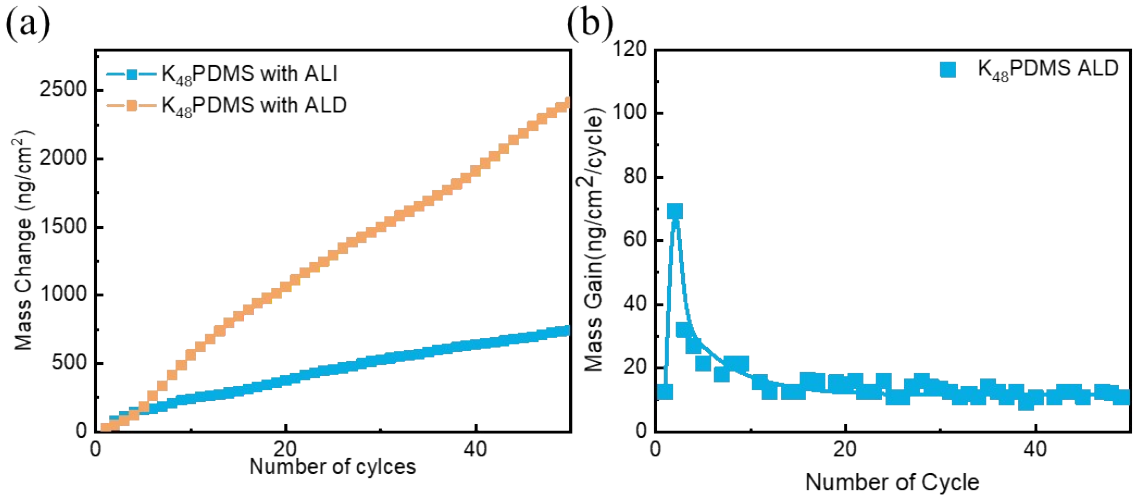

Figure S13. QCM analysis. (a) Mass uptake per cycle on K_{48}PDMS for the ALD process. (b) The total mass gain on K_{48}PDMS for both ALD and ALI processes in the 50 cycles

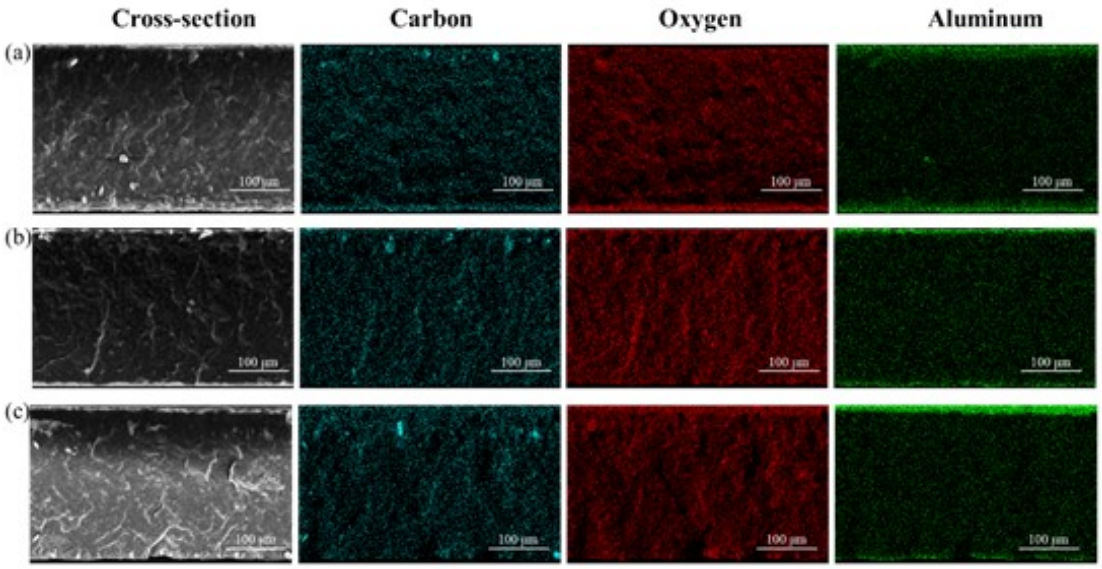

Figure S14. Cross-sectional SEM images and corresponding EDS maps of K_nPDMS with ALI cycle of 100 cycle. (a) K_{32}PDMS, (b) K_{48}PDMS, (c) K_{64}PDMS.

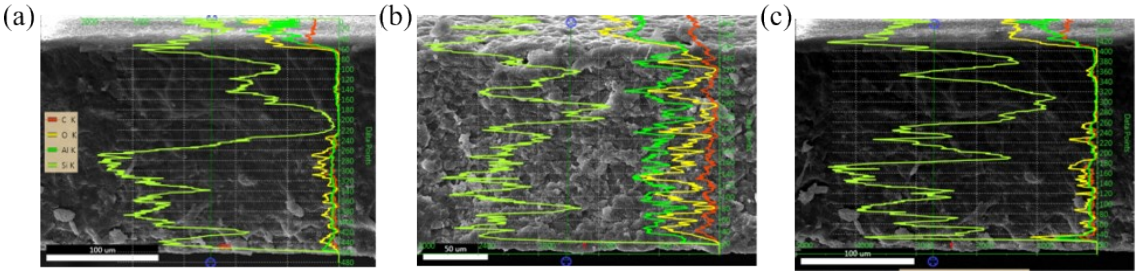

Figure S15. The SEM images of K_nPDMS treated with ALI in element line scan analysis. (a) K_{32}PDMS, (b) K_{48}PDMS, (c) K_{64}PDMS.

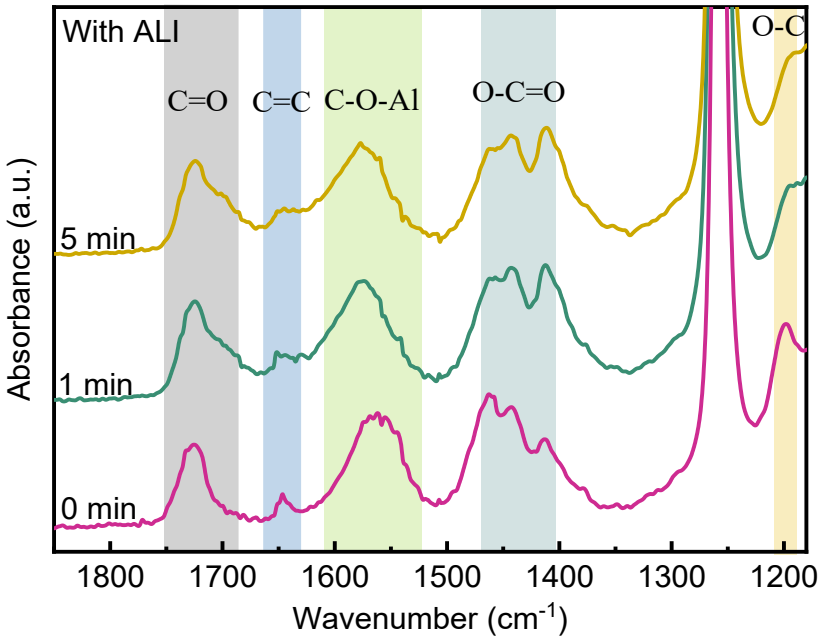

Figure S16. FTIR of K_{48}PDMS after UV-curing with ALI process.

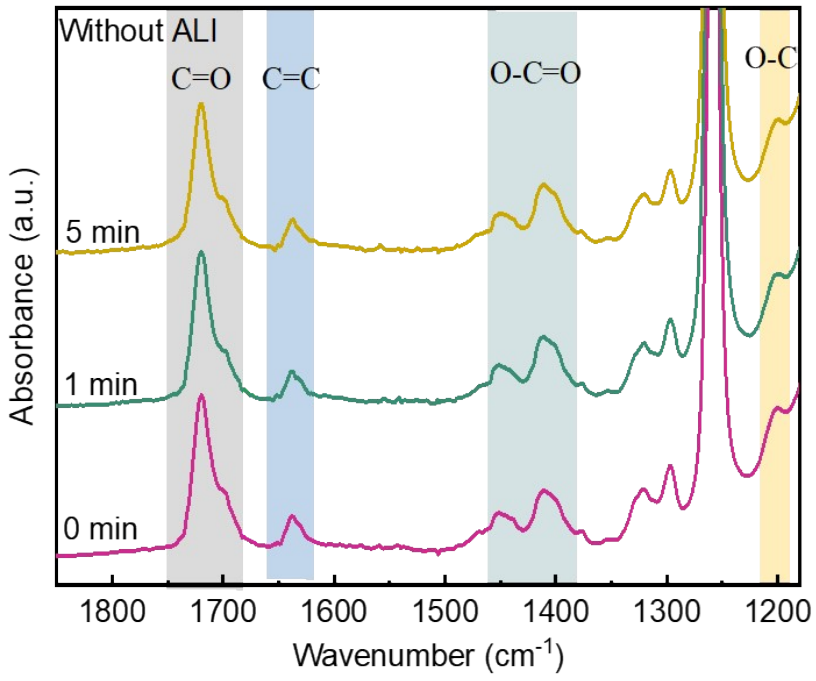

Figure S17. FTIR of K_{48}PDMS after UV-curing without ALI process.

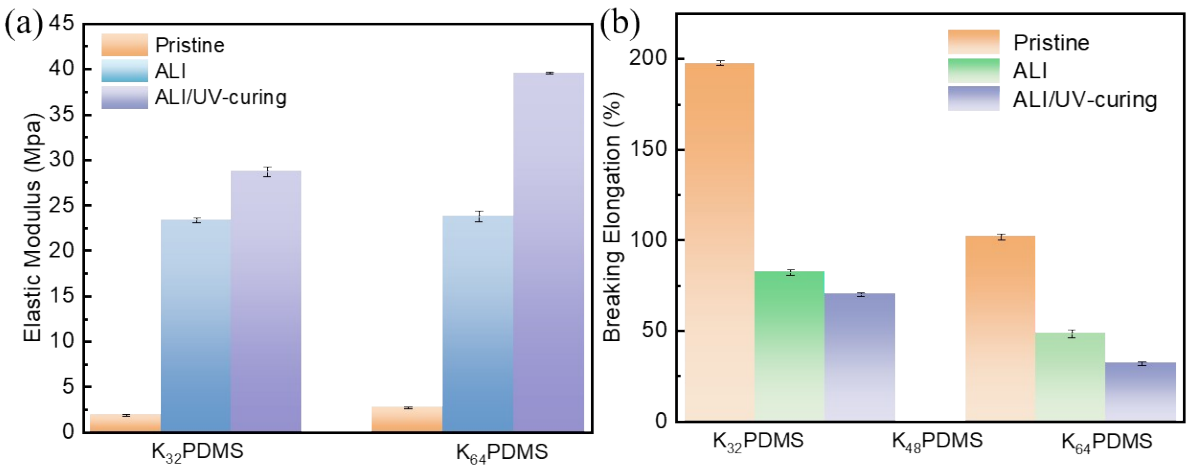

Figure S18. Elastic Modulus and Breaking Elongation of K_nPDMS (n=32, 64).

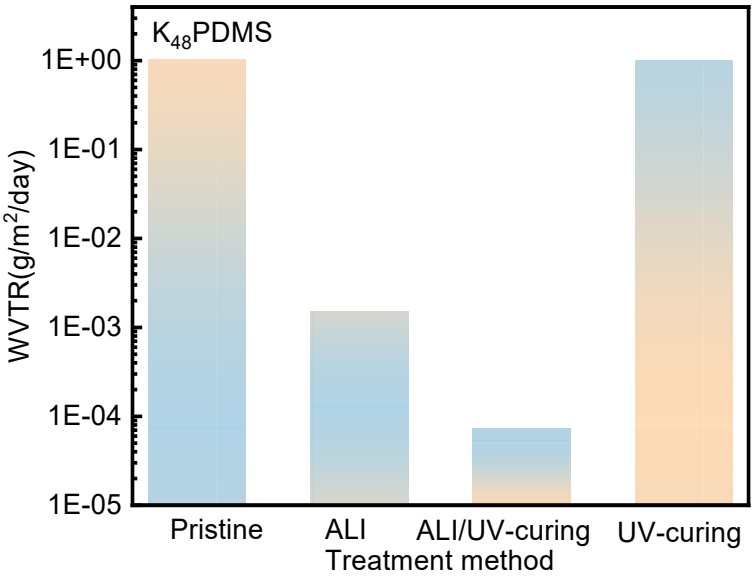

Figure S19. Barrier properties of pristine K_{48}PDMS and K_{48}PDMS treated with UV-curing, ALI, and the combined ALI/UV-curing process.

Table S1 Barrier properties, flexibility of various types of barriers

Deformation	Material	Bending radius	Strain	WVTR ($g/m^{-2}/day$)	WVTR after deformation	Resistance in PBS	Ref.
Stretching	$K_{48}PDMS/Al_2O_3$		1%	7.30×10^{-5}	7.82×10^{-5}	115 h	This work
	Al_2O_3/2LG/PI		1%	3.85×10^{-1}	3.85×10^{-1}	-	1
	$PDMS/SiO_2/Al_2O_3$		1%	1.81×10^{-3}	2.01×10^{-3}	-	2
Bending	PET/Al_2O_3/Ag/ Al_2O_3/S-H	30 mm	0.41%	8.70×10^{-6}	4.46×10^{-5}	-	3
	PET/PHPS/PVA	30 mm	0.23%	2×10^{-2}	2×10^{-2}	-	4
	PET/ double-sided a-SiNx:H	25 mm	0.25%	3.8×10^{-4}	1.08×10^{-3}	-	5
	PET/ a-SiNx:H/ n-SiOxNy/h-SiOx	25 mm	0.25%	9.2×10^{-5}	5×10^{-5}	-	
	PET/sub/buffer/ barrier	24.3 mm	0.10%	3.34×10^{-3}	3.34×10^{-3}	-	6
	PET/alumina	20 mm	0.31%	3.21×10^{-4}	1.69×10^{-3}	-	7
		10 mm	0.63%		8.07×10^{-4}	-	
	PEN/ZnO/ Al_2O_3/MgO	7 mm	0.89%	2.44×10^{-6}	2.65×10^{-5}	-	8
	PEN/ Al_2O_3	7 mm	0.89%	7.59×10^{-5}	6.97×10^{-3}	-	9
	PEN/SiN_x/ Al_2O_3	15 mm	0.42%	5.93×10^{-4}	3.97×10^{-4}		
	PET/Al_2O_3/ MgO	10 mm	0.63%	1.7×10^{-5}	6.9×10^{-5}	-	10
	PET/Nano-stratified /organic layer	10 mm	0.63%	1.77×10^{-5}	1.35×10^{-2}	-	
	PET/Al_2O_3/organic layer	10 mm	0.63%	7.87×10^{-6}	7.78×10^{-5}	-	11
	PET/polysilazane	5 mm	0.50%	2.7×10^{-4}	1×10^{-3}	-	12
	PI/Al_2O_3/Alucone	3 mm	0.83%	8.24×10^{-5}	6.06×10^{-4}	-	13
	PET/thin film barrier	7.5 mm	0.33%	3.12×10^{-4}	1.33×10^{-3}	-	14
		5 mm	0.50%		2.9×10^{-3}	-	
	PEN/Al_2O_3/Alucone	3 mm	-	1.18×10^{-5}	1.23×10^{-5}	-	15
	PEN/Al_2O_3/Alucone	3 mm	-	1.44×10^{-5}	1.37×10^{-5}	-	16
	PI/Al_2O_3	1.75 mm	0.29%	10^{-5}	10^{-5}	-	17

Table S2 Literature summary of resistance to PBS solution for various barriers

Material	Flexibility	Resistance in PBS	
KPDMS/Al_2O_3	**1%**	**115h**	This work
ZnO_2	-	8 h	[18]
PLGA/PVA/Al_2O_3	-	32 h	
HfO_2	-	1.33h	
SiNx/Al_2O_3/Parylene C	-	62.5 h	[19]
Parylene C/Al_2O_3	-	12 h	
PI/HfO_2	-	10 h	
SiO_2/SiN_x	-	60 h	[20]
HfO_2/t-SiO_2	-	84 h	[21]
Parylene C/Al_2O_3	-	96 h	[22]
Al_2O_3	-	48 h	[23]

Reference

1 S. Won, D. Van Lam, J. Y. Lee, H. J. Jung, M. Hur, K. S. Kim, H. J. Lee and J. H. Kim, *Nanotechnology*, 2018, **29**, 125705.

2 Y. Zhang, D. Wen, M. Liu, Y. Li, Y. Lin, K. Cao, F. Yang and R. Chen, *Adv. Mater. Interfaces*, 2022, **9**, 1–9.

3 J. H. Kwon, S. Choi, Y. Jeon, H. Kim, K. S. Chang and K. C. Choi, *ACS Appl. Mater. Interfaces*, 2017, **9**, 27062–27072.

4 I. A. Channa, A. Distler, M. Zaiser, C. J. Brabec and H. J. Egelhaaf, *Adv. Energy Mater.*, 2019, **9**, 1–10.

5 K. Y. Lim, D. U. Kim, J. H. Kong, B. Il Choi, W. S. Seo, J. W. Yu and W. K. Choi, *ACS Appl. Mater. Interfaces*, 2020, **12**, 32106–32118.

6 K. W. Lu, H. L. Chen, H. P. Chen and C. C. Kuo, *Thin Solid Films*, 2023, **767**, 139672.

7 J. H. Woo, D. Koo, N. H. Kim, H. Kim, M. H. Song, H. Park and J. Y. Kim, *ACS Appl. Mater. Interfaces*, 2021, **13**, 46894–46901.

8 J. H. Kwon, Y. Jeon, S. Choi, J. W. Park, H. Kim and K. C. Choi, *ACS Appl. Mater. Interfaces*, 2017, **9**, 43983–43992.

9 J. S. Park, S. H. Yong, Y. J. Choi and H. Chae, *AIP Adv.*, , DOI:10.1063/1.5037953.

10 K. S. Kang, S. Y. Jeong, E. G. Jeong and K. C. Choi, *NANO Res.*, 2020, **13**, 2716–2725.

11 E. G. Jeong, S. Kwon, J. H. Han, H.-G. G. Im, B.-S. S. Bae and K. C. Choi, *Nanoscale*, 2017, **9**, 6370–6379.

12 H. I. Lu, D. P. Tran, C. K. Lin and B. D. To, *Coatings*, , DOI:10.3390/coatings8040127.

13 J. H. Han, T. Y. Kim, D. Y. Kim, H. L. Yang and J. S. Park, *Dalt. Trans.*, 2021, **50**, 15841–15848.

14 D. P. Tran, C. K. Lin and B. D. To, *Thin Solid Films*, 2018, **650**, 20–31.

15 Z. Wang, Z. Chen, J. Wang, L. Shangguan, S. Fan and Y. Duan, *Opt. Express*, 2023, **31**, 21672.

16 Z. Wang, J. Wang, Z. Li, Z. Chen, L. Shangguan, S. Fan and Y. Duan, *Nano Energy*, , DOI:10.1016/j.nanoen.2023.108232.

17 S. H. Kim, S. Y. Song, S. Y. Kim, M. W. Chang, H. J. Kwon, K. H. Yoon, W. Y. Sung, M. M. Sung and H. Y. Chu, *npj Flex. Electron.*, 2022, **6**, 1–6.

18 S. Huang, W. Xuan, S. Liu, X. Tao, H. Xu, S. Zhan, J. Chen, Z. Cao, H. Jin, S. Dong, H. Zhou, X. Wang, J. M. Kim and J. Luo, 2019, 22369–22377.

19 E. Song, J. Li and J. A. Rogers, *APL Mater.*, , DOI:10.1063/1.5094415.

20 E. Song, Y. K. Lee, R. Li, J. Li, X. Jin, K. J. Yu, Z. Xie, H. Fang, Y. Zhong, H. Du, J. Zhang, G. Fang, Y. Kim, Y. Yoon, M. A. Alam, Y. Mei, Y. Huang and J. A. Rogers, *Adv. Funct. Mater.*, 2018, **28**, 1–10.

21 E. Song, R. Li, X. Jin, H. Du, Y. Huang, J. Zhang, Y. Xia, H. Fang, Y. K. Lee, K. J. Yu, J. K. Chang, Y. Mei, M. A. Alam, Y. Huang and J. A. Rogers, *ACS Nano*, 2018, **12**, 10317–10326.

22 H. Fang, J. Zhao, K. J. Yu, E. Song, A. B. Farimani, C. H. Chiang, X. Jin, Y. Xue, D. Xu, W. Du, K. J. Seo, Y. Zhong, Z. Yang, S. M. Won, G. Fang, S. W. Choi, S. Chaudhuri, Y. Huang, M. A. Alam, J. Viventi, N. R. Aluru and J. A. Rogers, *Proc. Natl. Acad. Sci. U. S. A.*, 2016, **113**, 11682–11687.

23 C. Li, M. Cauwe, Y. Yang, D. Schaubroeck and L. Mader, *Coatings*, 2019, **9**, 579.